







Experimental and Numerical Study of Maximum Welding Joint Temperature Impacts in Alloy Steel Pipe Welding Microstructure, Distortion, Corrosion Resistance, and Mechanical Properties

Samir Ali Amin¹, Ayad Abbood Abdulhasan², Mohammed Sabeeh Mohammed^{3*}, Hasan Shakir Majdi⁴

¹ Engineering of Refrigeration and Air-conditioning Techniques, College of Engineering Techniques, Al-Farahidi University, Baghdad 10017, Iraq

² Department of Metallurgy Engineering, Al-Mustafa University College, Baghdad 10023, Iraq

³ Training and Workshop Center, University of Technology- Iraq, Baghdad 1006, Iraq

⁴ Department of Chemical Engineering and Petroleum Industries, Al-Mustaqbal University College, Hillah 51001, Iraq

Corresponding Author Email: mohammed.s.mohammed@uotechnology.edu.iq

Copyright: ©2024 The authors. This article is published by IETA and is licensed under the CC BY 4.0 license (<http://creativecommons.org/licenses/by/4.0/>).

<https://doi.org/10.18280/rcma.340612>

ABSTRACT

Received: 18 March 2024

Revised: 20 July 2024

Accepted: 19 November 2024

Available online: 28 December 2024

Keywords:

FE models, ANSYS, SolidWorks, polygonal ferrite, Widmanstatten ferrite

This study investigates how welding currents influence maximum temperature exchange cross welding joints. The study also examines how these modifications impact the alloy steel pipe welding deformation, corrosion resistance, microstructure, and mechanical properties. This study utilizes numerical models and experimental methods using finite element (FE) technique. Study used SolidWorks software program to generate three-dimensional thermo elastic-plastic finite element models. ANSYS software used to analyze a simulation model, including a double-ellipsoidal heat source model, material properties dependent on temperature, and the influence of geometric parameters. The finite element models' correctness was validated by comparing simulation results and empirically obtained data. Both computational techniques and observations indicate that higher maximum welding joint heat substantially affects the development of distortion, change of microstructure, and the resulting impact on joint corrosion resistance. The numerical findings of this research are significant for comprehending the precision needed to capture welding process's essential intricacies. From welding engineering perspective, this work's conclusions are relevant. They demonstrate transverse residual stress fields caused by short fillet welds concentrated in certain areas and have much higher peak magnitudes than continuous pipe welds.

1. INTRODUCTION

Welding creates solid and seamless metallic connections between different metallic components. As mentioned before, welding involves using heat energy to fuse two materials. The required temperature and force for the fusion of two materials may vary greatly depending on whether heat or pressure alone is used. Heat is used only to form the junction, whereas pressure is employed primarily to keep joining parts nearby. Three examples of this process are shielded metal arc welding (SMAW), gas tungsten arc Welding (GTAW), and submerged arc welding (SAW). SMAW is the oldest of all arc welding methods. It is characterized by its capacity to adjust, directness, and flexibility. Shielded metal arc welding (SMAW) technique often used for tack welding, diverse components fabrication, and welding repairs [1].

The primary motivation for studying welding is to overcome weldment flaws and limitations associated with welding as vital joining process. Expected subjecting metals' negative consequences to welding conditions and subsequent solidification encompass material distortion, mechanical

properties deterioration in welding region caused by induced residual stresses, and other factors associated with observed modification in microstructure [2]. Materials in a state other than equilibrium have beyond their melting temperature. Convective processes occur inside the liquid pool, enhancing the transfer of heat. The metal undergoes solidification upon cooling when the heat sources are eliminated. Temperature variations in the alloy throughout the cooling process lead to solid-state transitions [3, 4]. The microstructural modifications change the material characteristics as the process progresses. The heat strains around the welding area are elastoplastic, leading to stresses that result in permanent distortions. These distortions also impact the dimensional integrity of the joint [5, 6]. To assess the weld joint, it is necessary to conduct mechanical testing and a thorough metallographic inspection to analyze the microstructural variations in the weld area [7, 8]. Previous research allowed the fast progress of welding methods, welded materials thermo mechanical properties comprehensive analysis, and welding defect efficient solutions, thereby reducing the main obstacles [9, 10]. The matter of welding gets intricate when the base metals or alloys display

localized disparities in their chemical compositions, such as distinct metals or different versions of the same metal. These differences occur because of changes in thermo-mechanical properties [11]. Previous research focused on enhancing welding processes or technologies that could effectively tackle critical concerns such thermal instability, non metallic (oxide) particles in fusion zone, corrosion resistance, and difficulties associated with metal alloys and filler materials compatibility. Thorough research has effectively addressed these problems over many years [12, 13]. Current research focuses on enhancing the efficiency of welding operations by conducting extensive investigations into weld flaws beyond the fusion zone (FZ). An ongoing concern for academics is reducing the expenses of metal heat treatment. This process is crucial for restoring key mechanical characteristics of welded materials [14]. Conventional analytical methods for addressing issue often complex and sometimes difficult to execute. Among other numerical methods, finite element technique has widely used for heat profiling in welding process. Advanced numerical simulation and welding modeling were done by Grubits et al. [15] their research explains new techniques in this field with good results. Developed three-dimensional (3D) finite element (FE) analysis performed by Moslemi et al. [16] to generate thirty sets of normalized input (welding pool characteristics) and outputs (Goldak's parameters) to novel systematic numerical approach heat source parameters determination in welding.

Finite element method (FEM) often requires repeated mesh adjustments when simulating protracted distortions in material flow to ensure accurate outcomes. The mesh free techniques provide advantages by obviating the need for conventional finite element (FE) mesh or grid structure to discretize problem. Smoothed Particle Hydrodynamics (SPH) is one of the often-used mesh-free methods [16]. Two methods mentioned are Element-Free Galerkin (EFG) [17] and Radial Basis Function (RBF) [18]. Conventional welding involves incorporating a heat model connected to a trainset and a static structure modeling process. Commercially accessible software applications, such as ANSYS, may use to analyze thermal elastic plastic stresses and distortion in welding using finite element method (FEM). The finite detail evaluation of welding residual stresses entails thinking about different factors, such as the temperature-based non-linear behavior of materials, weld pool three-dimensional nature, and welding methods and section transitions impacts because of alterations in welding joint and HAZ microstructure. This article utilizes the ANSYS and SolidWorks software to do a finite detail simulation of heat distribution and deformation in low alloy metallic pipe welding. The choice of material for the pipe welding is alloy steel. This cloth has many uses in constructing systems and parts, inclusive of bridges, metallic systems, and industrial machine components. An analysis is carried out on the 3D finite detail version, resulting in the acquisition of the temperature distribution and deformation.

Thus, this study shows a complete examination of the thermal and mechanical residences of weld in alloy metallic storage tank shells. This might consist of developing an appropriate numerical model to investigate the structural deformation and heat distribution. Furthermore, thoroughly examining the intricate structural changes and nucleation processes involved in heat dissipation during welding is necessary to manage weld defects effectively and prevent the deterioration of the material's mechanical properties. This analysis should encompass the entire heat-affected zone, from

the welding fusion zone to base metal, to ensure the creation of highly dependable joints with desirable mechanical characteristics.

2. EXPERIMENTAL METHOD

Two alloy steel pipes were welded together in the butt position with a single V joint. The welding joint designed according to AWS D1.1 standards, and with one pass of SMAW technology, welding parameters listed in Table 1. The welding pipe samples have 80 mm outer diameter and 72 mm inner diameter. Three samples with three heat input values resulting from the change in welding current estimated according to Eq. (1) were welded in this study to analyze the welding heat alteration effects on HAZ and fusing joint microstructures, mechanical properties, and corrosion resistance.

$$H = \frac{VI}{1000S}(\text{Joule/mm}) \quad (1)$$

where, H = heat input (joule/mm), V = arc voltage (volts), I = current (amps), and S = welding speed (mm/min).

Welding joint maximum temperature for SMAW calculated according to Eq. (1) results following the equation:

$$T \text{ max} = (H \times 0.4) + T_o \quad (2)$$

where, T max = welding joint maximum heat temperature (°C), H = heat input (joule/mm), and T_o = base metal temperature before welding (°C).

Table 1. Three samples of welding parameters

Samples No.	Welding Current (A)	Welding Speed (mm/min)	Heat Input (Joule/mm)	Max. Joint Temp. (°C)
W1	213	75	6195	2500
W2	170	75	4945	2000
W3	152	75	4445	1800

After the welding, the samples are prepared for the microstructure examination by grinding them to 2000 grid paper degrees and then polishing them to the mirror face; then cleaning the samples after polishing them with acetone to remove any dirt before optical examination. After cleaning, the testing samples were etched with 2cc HNO₃ + 98cc Ethyl alcohol (Nital (2%)).

(OPTIKA B-383MET - Metallurgical Microscope) was used to examine the welding joint and the HAZ microstructure. Tensile testing is conducted on extracted tensile samples obtained from weldments. Samples are extracted using wire cut electric discharge machining in of the pipe joints transverse direction, following standard dimensions specified in American Society of Mechanical Engineers (ASME) section IX standards [19], shown in Figure 1. The tensile testing uses a universal testing machine (HLY-1000KN Hydraulic Universal Testing Machine model) that has 1 mm/min crosshead travel speed. The SEM equipment from ZEISS examines the broken tensile surfaces thoroughly. Microhardness test performed using hardness measurement tester, specifically NEXUS 4302 model of ESEWAY machine. In this test, 300 g force applied to create indentation, and measurements taken at 100 μm intervals.

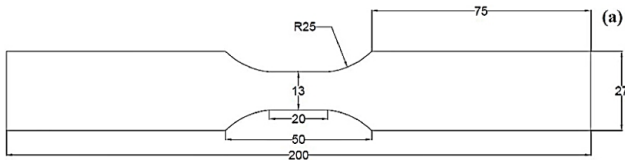


Figure 1. Tensile test sample dimensions

3. NUMERICAL SIMULATION OF THE WELDING JOINTS

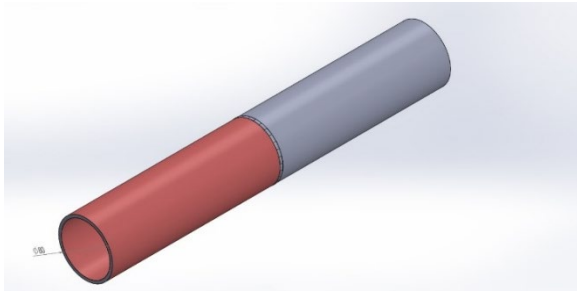


Figure 2. SolidWorks pipe joint design

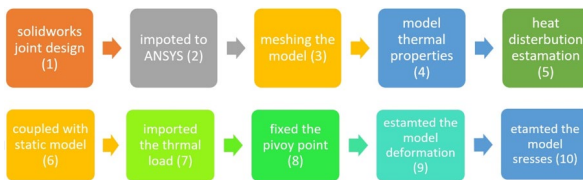


Figure 3. Two stages simulation procedure

Welding simulation's first stage involves weldments and joint design creation. These refer to three welding heat input joints used in specific applications for manufacturing alloy steel pipe weldments. Welding joint design executed using SolidWorks software. V shaped joints with a root spacing of 1.6 mm were developed for this investigation. The weldments are constructed with 4 mm pipe wall thickness and 250 mm length. Both joint sides had 80 mm outside diameter as illustrated in Figure 2. Welding joint design has tiny, uniform sections to replicate the motion of arc welding technology along the joint. The 3D thermo-mechanical finite element model of SolidWorks was imported into ANSYS to accurately forecast the thermal, deformation, and residual stresses of joint welding temperature profiles during the three welding heat processes. Functional equivalence (FE) analysis was conducted systematically using the technique outlined in Figure 3. Initially, welding process thermal analysis conducted to test heat distribution in welding joints due to applied input heat. Subsequently, thermal and experimental load analysis was used to execute static analysis and predict stress distribution and deformation in welded joints. Several assumptions made throughout thermal and static investigations conducted. Base material's ambient temperature assumed 22°C before welding. Alloy steel selection as simulation material based on its compatibility with various applications and favorable mechanical and physical qualities.

4. SIMULATION MODEL MESHING

Meshing is a crucial element of engineering simulation process. In order to ensure simulation precision, high fidelity

mesh generated essential to methodically due to its paramount significance. Creating optimal mesh crucial during engineering simulations due to its influence on simulation's accuracy, convergence, and efficiency. Computer cannot perform simulations on CAD model physical shape because they cannot apply governing equations to geometry, which is not well-defined. Mesh element allows governing equations resolution on volumes with specified geometries and mathematically defined. Typically, equations solved on these meshes partial differential equations. Given these computations repetitive nature, it's not feasible to solve these equations manually. Therefore, computer approaches such finite element analysis (FEA) used. The meshing procedure used an ANSYS mesh configuration to achieve mesh elements' optimal distribution for welding joint geometry approach. Standard metal set 6 mm beginning thickness. V joint with 5 mm elements dimensions, with root gap joint used in this simulation, mesh using 66494 nodes and 32084 elements. Simulation models meshed using welding joint multizone approach and tetrahedrons for weldment remaining parts, as demonstrated in Figure 4. Current study used SolidWorks dimensions to construct and physically simulate single V welding pass joint design in vertical joint. Three experimental samples fabricated and joined to compare deformation results obtained from ANSYS model with actual deformation observed to enhance realism and validate simulation model findings.

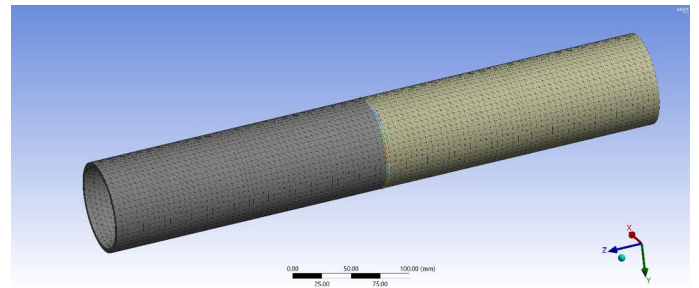


Figure 4. ANSYS mesh for the joint and base metal

5. WELDING SIMULATION THERMAL ANALYSIS

Analyzing heat transmission in welding involves examining a dynamic process regulated by a well-recognized heat conduction equation.

$$\rho c \frac{\partial T}{\partial t}(x, y, z, t) = \nabla \cdot \vec{q}(x, y, z, t) + G(x, y, z, t) \quad (3)$$

The variables in the equation are as follows: ρ represents material density, c represents specific heat capacity, T represents instantaneous temperature, \vec{q} represents heat flow vector, G represents internal heat production rate, x , y , and z represent coordinates in reference system, t represents time, and ∇ means spatial gradient operator. Viewing the system as a three-dimensional plate with X , Y , and Z coordinates, heat source path situated on the $z = 0$ surface.

$$\vec{q} = -k \nabla T \quad (4)$$

The equation for transient heat conduction in a stationary medium may state in extended form as a three-dimensional equation.

$$\rho c \frac{\partial T}{\partial t} = \frac{\partial}{\partial x} \left(k_x \frac{\partial T}{\partial x} \right) + \frac{\partial}{\partial y} \left(k_y \frac{\partial T}{\partial y} \right) + \frac{\partial}{\partial z} \left(k_z \frac{\partial T}{\partial z} \right) + G \quad (5)$$

T represents the current temperature, whereas k_x , k_y , and k_z represent the thermal conductivities in the x, y, and z directions, respectively. The flux boundary conditions at the top surface ($z = 0$) are determined by a heat source traveling at a constant velocity, v_x , along the x-axis. These conditions can be described using a Gaussian function.

$$Q_{max} = \frac{AQ}{\pi r_0^2} \quad (6)$$

Q_{max} heat flux at heat source center, r_0 heat source distribution radius, Q heat source power, and A constant called arc concentration coefficient. Convective boundary condition on workpiece surface given by:

$$q = k_x \frac{\partial T}{\partial x} n_x + k_y \frac{\partial T}{\partial y} n_y + k_z \frac{\partial T}{\partial z} n_z + h(T - T_\infty) \quad (7)$$

Let q denotes heat transferred to welding surface by welding arc. This heat is non-zero along the weld line and zero elsewhere on workpiece. The "h" symbol represents convective heat transfer coefficient, whereas " T_∞ " represents ambient temperature. Temperature profile is determined by calculating Eq. (3) concerning starting condition Eq. (4) and boundary conditions specified in Eqs. (3) to (7). At this juncture, the answer may be further explored via an analytical or numerical approach. This work proposes numerical Finite Element Method (FEM) using to calculate transient temperature distribution.

6. WELDING SIMULATION MECHANICAL ANALYSIS

Mathematical models and numerical analysis essential when welding joint deformation, thermal, elastic, plastic, and residual stresses needed to calculate and predict. Phase transformation takes place at comparatively low temperatures, allowing anticipating changes in microstructure, volume, and phase transformation inside welding joints and heat affected zone (HAZ) due to welding heat distribution patterns, and this will influence weld joint resultant mechanical characteristics. Temperature distribution computed and stored for each joint configuration during welding thermal analysis. This data then used as thermal loading to generate thermal stress field in mechanical analysis simulation. This enables thermal strains and stress computation over whole design. Thermal elastoplastic model uses Von Mises yield criteria and isotropic strain hardening rule. Simulation model stress to strain relations can mathematically represented:

$$\varepsilon_{total} = \varepsilon_e + \varepsilon_p + \varepsilon_t \quad (8)$$

To facilitate understanding of the equation, we articulate the constitutive equation in the following manner:

$$\sigma = D = D(\varepsilon_{total} - \varepsilon_p - \varepsilon_t) \quad (9)$$

The D matrix, representing material stiffness, simulated elastic plastic behavior, including linear kinematic hardening. For alloy steel, yield stress experiences substantial drop as temperature increases, ultimately ceasing to exist at melting point. Thermal load generated by three heat inputs applied to three joints welding zone. Weldment left and right sides fixed to replicate real life conditions. ANSYS determined Von Mises stresses, strain, and deformation resulting from this thermal load.

7. RESULTS AND DISCUSSIONS

7.1 Welding heat distribution and thermal analysis

A transient thermal study is conducted on a single V joint pipe utilizing various heat sources. The mobile welding heat input is regarded as a volumetric heat source. Filler material addition during welding replicated using element graduated heating approach [19]. Figure 5(A), (B), and (C) show temperature distribution at weldments from weld center line for different heat inputs. The figure depicts the maximum temperature reached by the nodes during welding process as heat source traverses its trajectory. As heat source approaches nodes, it reaches its maximum temperature; conversely, as heat source moves away, each node's temperature decreases. It also demonstrates that the welding process's cooling rate is comparatively slower than the heating rate. Figure 6(A) to (C) illustrate temperature distribution, fusion zone, and heat-impacted zone for different heat inputs. The red and orange regions in welding joint and adjacent heat affected zone (HAZ) indicate molten material presence with temperature over 1450°C. The borders of FZ may be readily anticipated based on the schematics in Figure 7(A), (B), and (C). Figures 5 and 6 demonstrate that increased heat input results in a larger weld pool and a broader heat affected zone (HAZ). Therefore, it is feasible in forecast pipe joint weld pool dimensions using simulation model like this. Also, from the exact figures, the calculated HAZ width of the first samples with 1800°C was 16.56 mm and 18.12 mm for the second sample with 2000°C and 21.64 mm for the third sample with 2500°C all the measurements calculated by ANSYS from the welding center line. These results proved direct relation between HAZ width and welding temperature. The temperature in estimated locations recorded by using probe tool in ANSYS software at fusion, and transformation temperature range to determine these zones' dimensions.

The calculation of the HAZ width was done by pointing the 723°C-region dimension from the welding center line; according to the Fe-C diagram, this the temperature is the transformation temperature where the solid structure transforms to γ (austenite); from this temperature and according to the welding input heat and cooling rate the final welding joint structure and its mechanical properties will be determined. For this reason, the dimension of this region is critical to fit the welding joint with the design criteria. The data required to draw the previous curves was calculated by recording the temperature values in a straight line from the welding edge to edge crossing the welding joint with snapping tool activation to ensure an equal distance between the recorded values, and then exporting these values to Excel sheet to generate the curves.

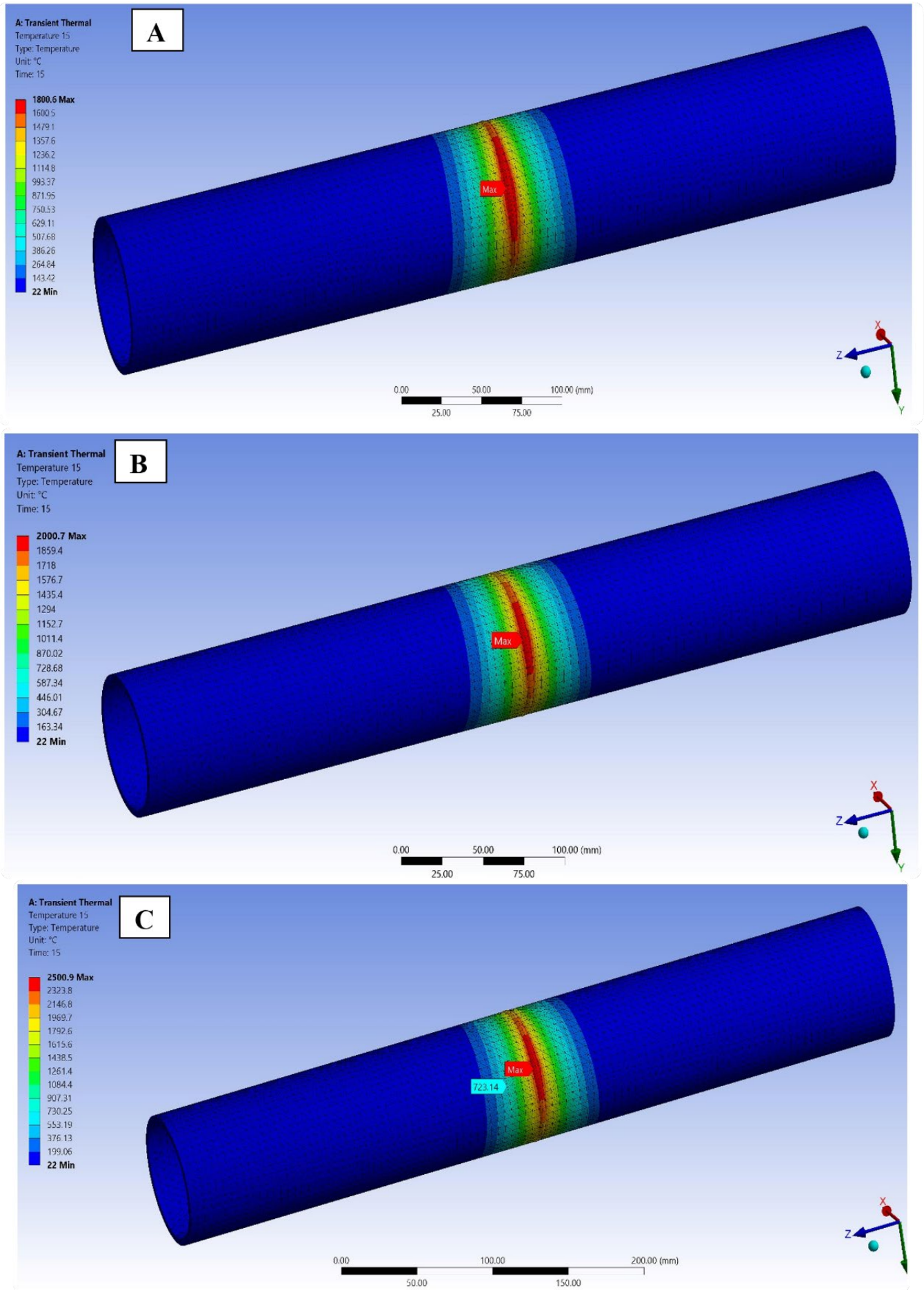


Figure 5. Welding heat distribution of the samples with (A) 1800°C, (B) 2000°C, and (C) 2500°C welding heat

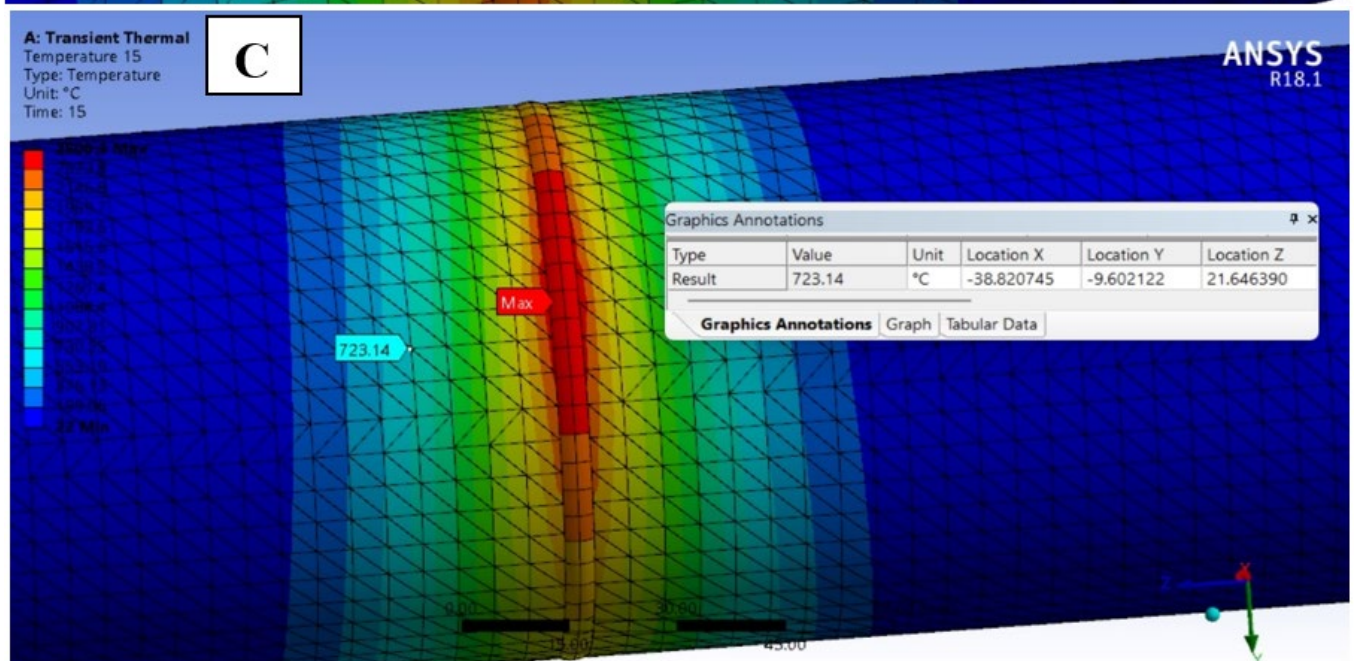
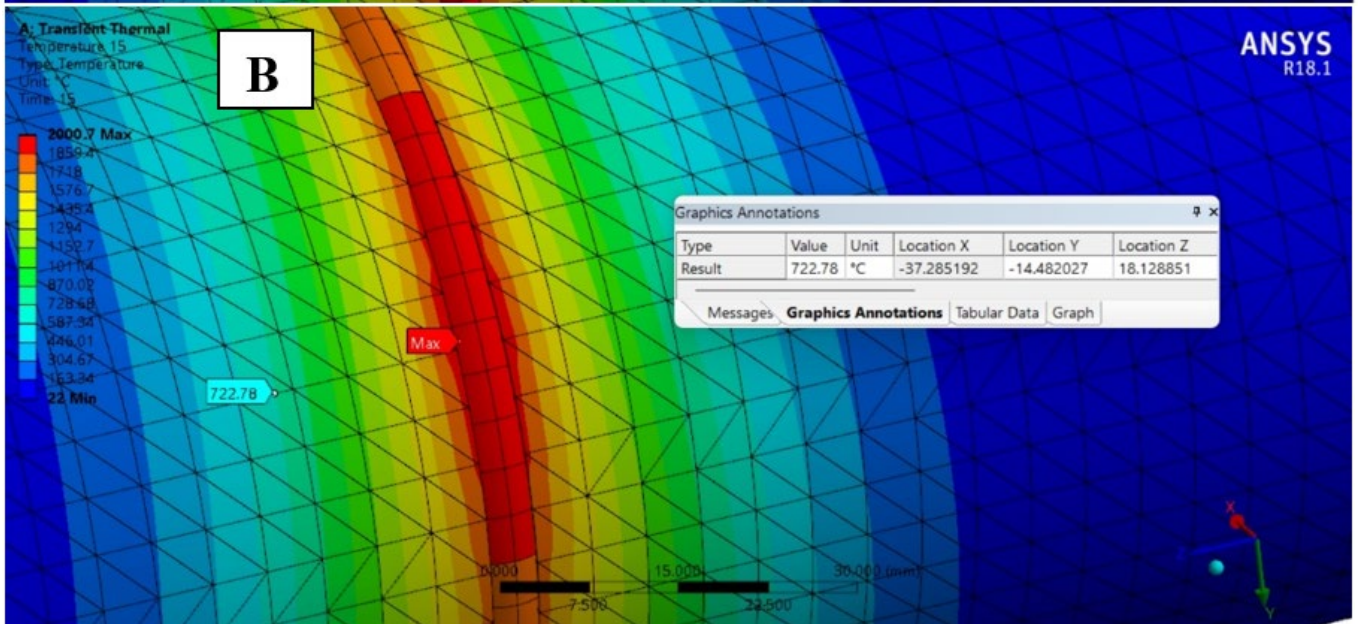
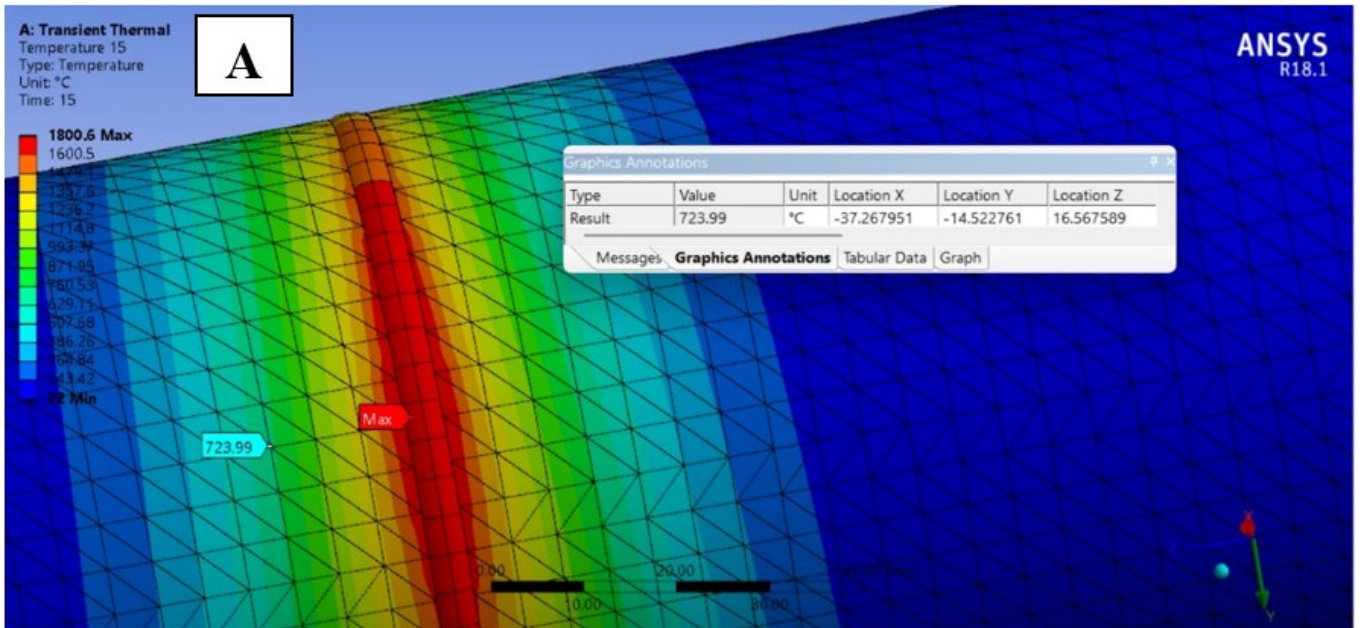


Figure 6. HAZ width dimensions of the samples with (A) 1800°C, (B) 2000°C, and (C) 2500°C welding heat

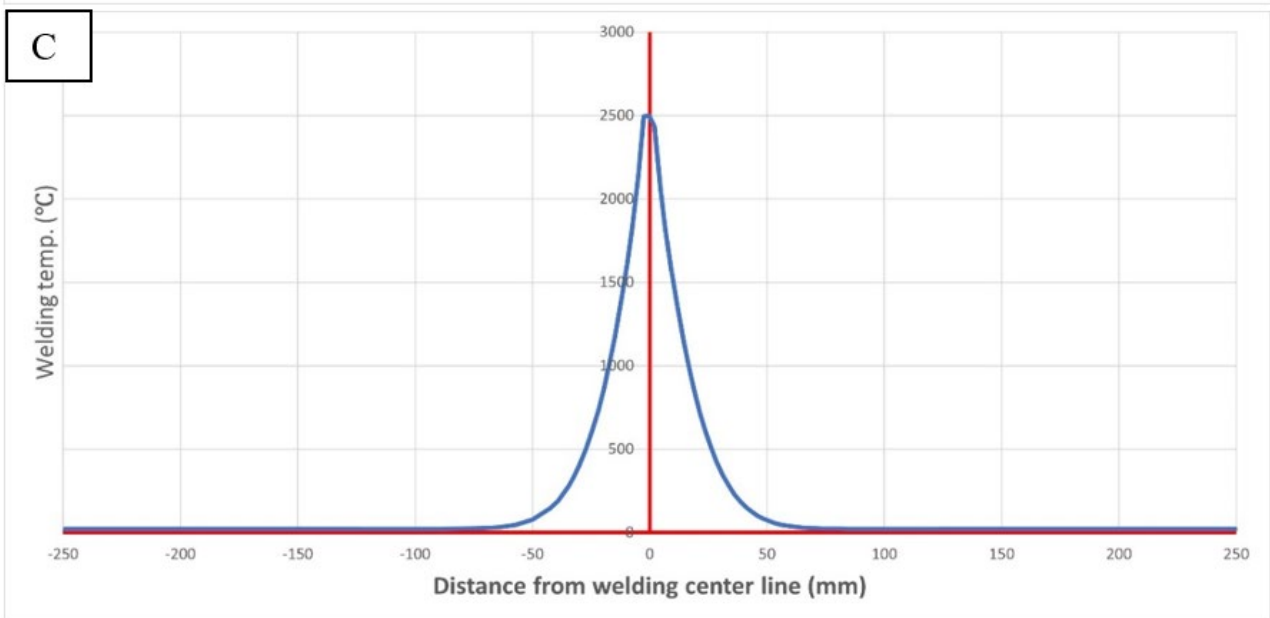
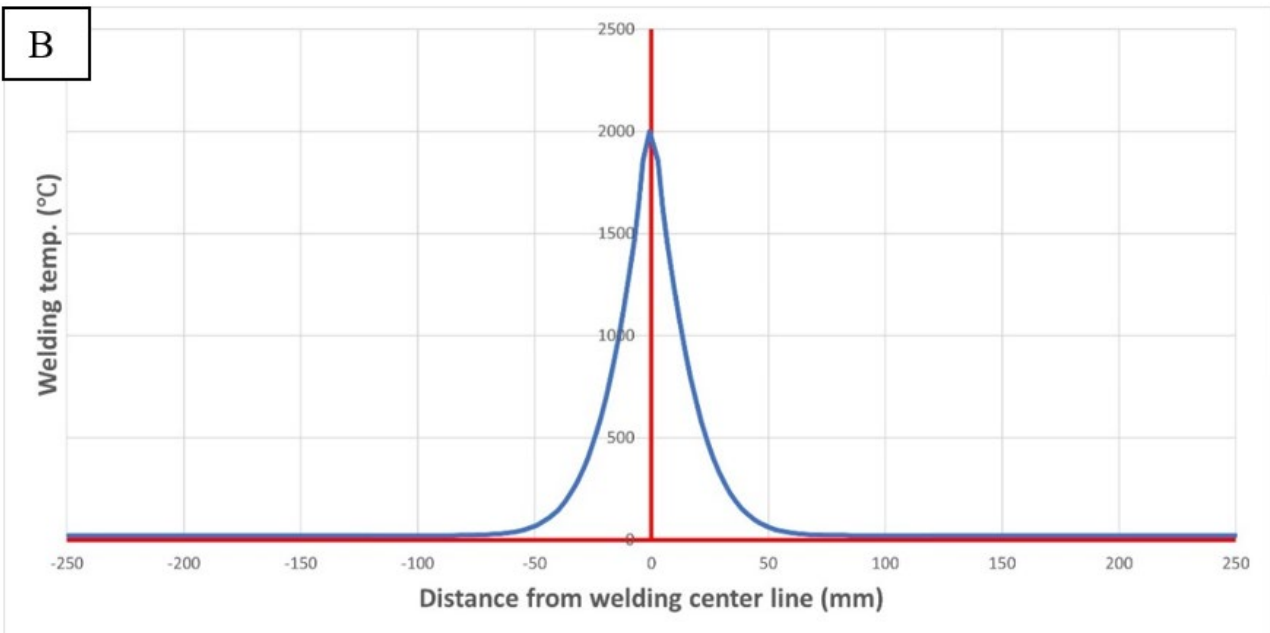
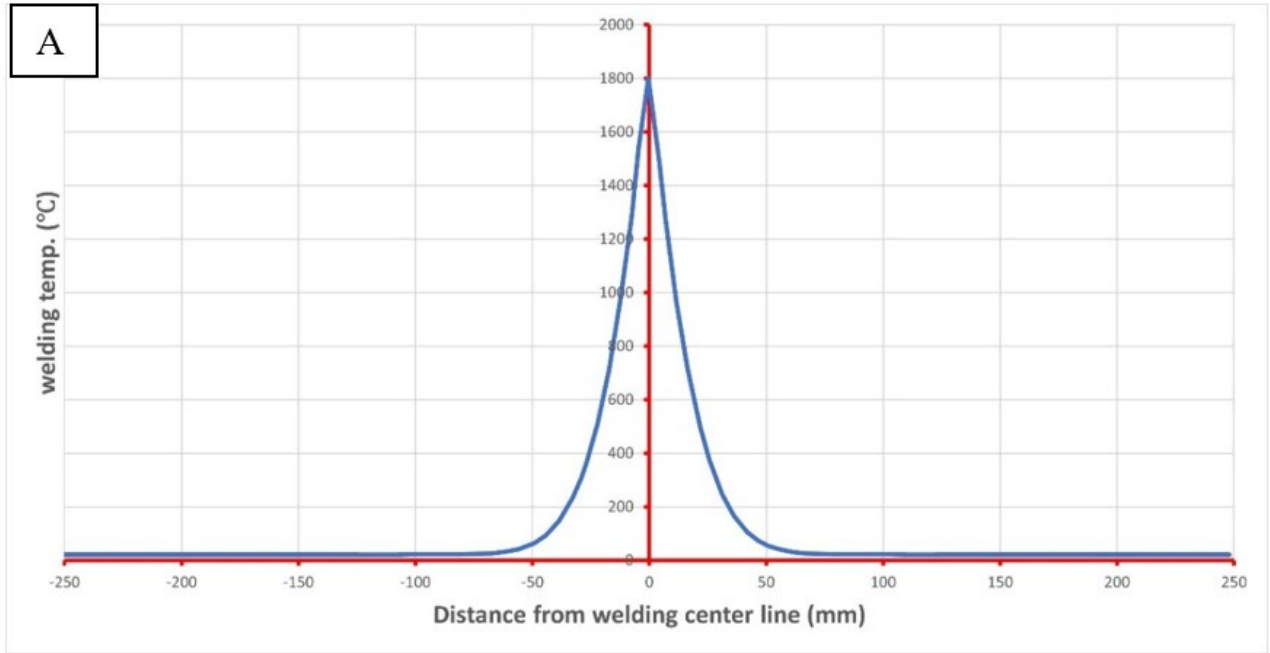


Figure 7. Welding heat distribution diagrams of the samples with (A) 1800°C, (B) 2000°C, and (C) 2500°C welding heat

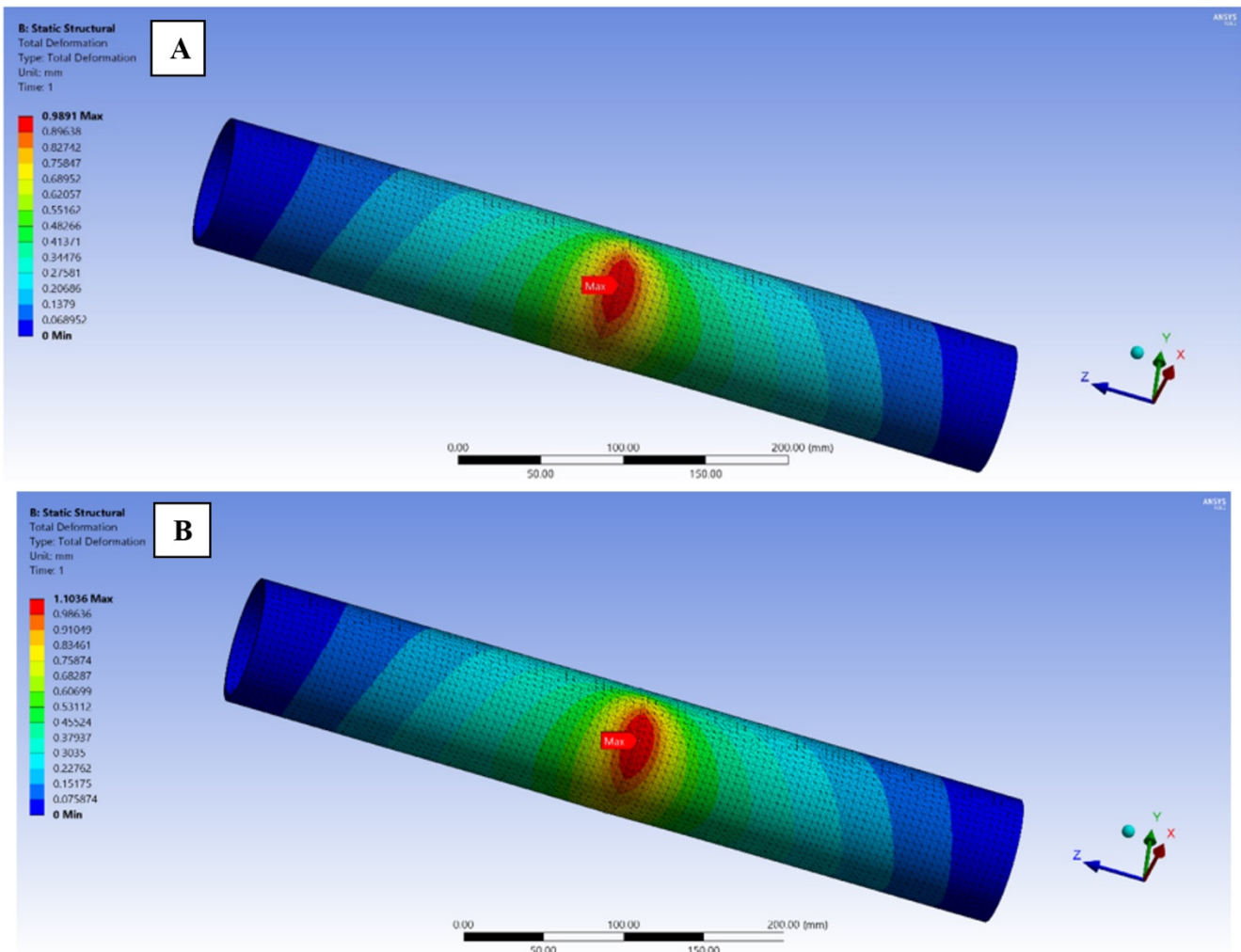
7.2 Welding deformation analysis

The input heat in alloy steel pipe welding is crucial in minimizing distortion. Welding generates heat that modifies the material's structure via recrystallization, grain development, and phase transition, a well-recognized occurrence. Alloy steel pipe is particularly susceptible to deformation during welding due to the base metal's unique properties and the impact of welding heat [20]. Upon completion of welding procedures, the material may undergo deformation, resulting in bending or shifting, often referred to as distortion. This distortion may cause issues for welded constructions due to its strength and functionality compromise.

Prior experimental findings indicate that the distortion of the welding joint may be minimized by using a V-shaped groove angle of 60° [21]. The distortion in single V groove butt weldment reduced as bevel angle increased due to difference in transverse shrinkage over specimen thickness. This research utilizes dynamic thermal source profile, namely deformation seen in heat flow directions under certain boundary circumstances. ANSYS simulation model in Figure 8(A), (B), and (C), reveal that pipe weldment welding joint end experienced 1.38 mm maximum deformation, which accounts for 34.5% of the pipe wall thickness and 1.72% of the pipe diameter when welded at a temperature of 2500°C . In comparison, the exact location of the weldment experienced a deformation of 1.10 mm, representing 27.5% of the pipe wall thickness and 1.37% of the pipe diameter when welded at a temperature of 2000°C . Furthermore, the weldment at a

maximum temperature of 1800°C exhibited a deformation of approximately 0.98 mm, about 24.4% of the pipe wall thickness and 1.22% of the pipe diameter. Notable disparity in deflection value across three models indicates how much welding joint distortion minimized, and standard dimensions aligned with design specifications.

The maximum deformation in all model's welding zones, as Figure 8 shows, is primarily caused by this area's prolonged exposure to high temperatures through welding. This exposure changes zone's properties, affecting its mechanical and thermal characteristics [22]. Around 800°C , latent heat amplifies specific heat and other phase transition characteristics. Thermal expansion ratio (TER) signifies comparison results from phase change. At temperatures over $600^\circ\text{C} - 700^\circ\text{C}$, yield stress becomes insignificant, or almost negligible. Material's flexibility and susceptibility to deformation heightened when yield stress almost absent. At this juncture, the substance exhibits characteristics like liquid and ceases to show resistance to deformation, referred to as mechanical melting point. Moreover, results demonstrated that fittings placement vital in determining zone where deformation effects occurred. Highest distortion zone in this investigation oriented towards connecting center line by securely fastening two welding edges and then releasing welding connection. The rationale for employing a moving heat source in this investigation was to simulate real-life welding conditions and ensure even distribution of heat and deformation across the welding joint.



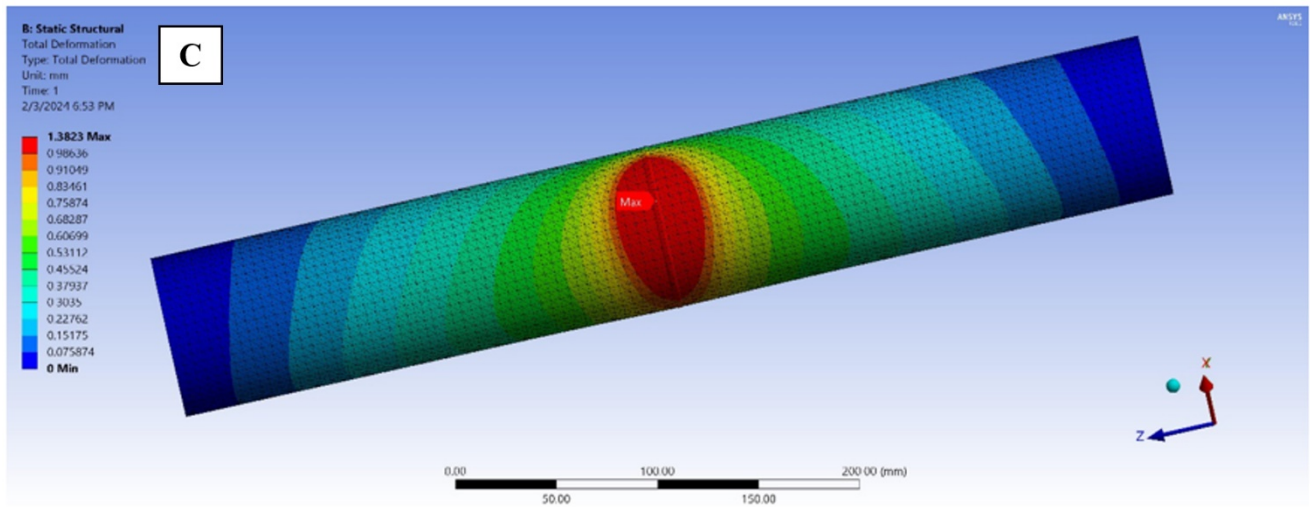


Figure 8. Welding joint deformation distribution of the samples with (A) 1800°C, (B) 2000°C, and (C) 2500°C welding heat

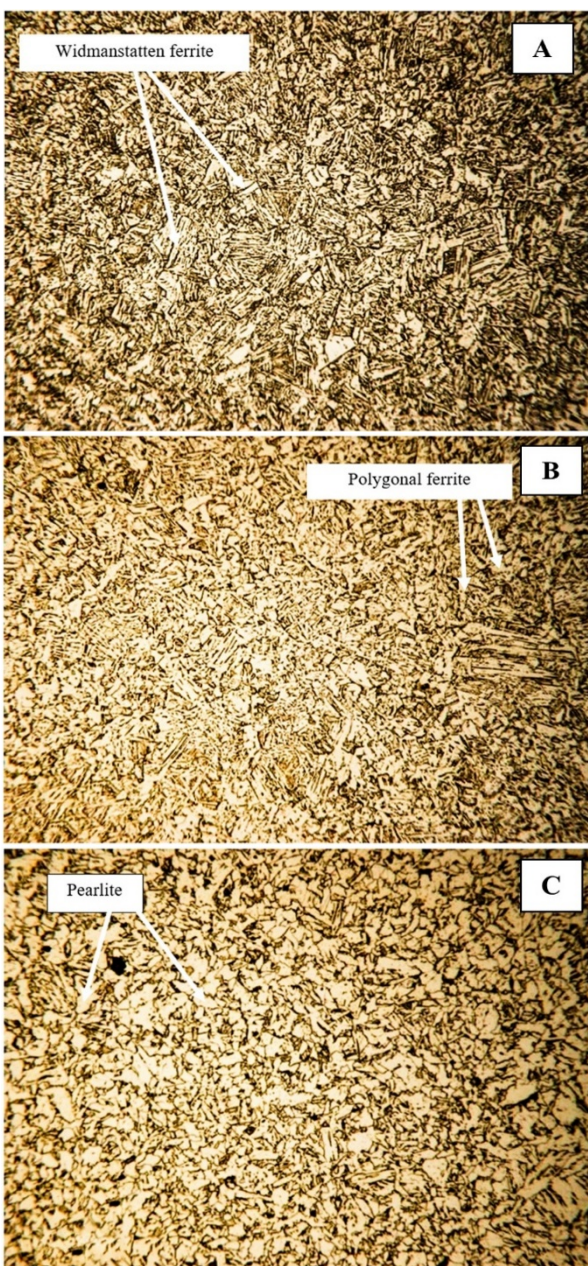


Figure 9. Welding joint microstructure of the samples with (A) 2500°C, (B) 2000°C, and (C) 1800°C welding heat

7.3 Welding joint microstructures analysis

The microstructure analysis of the three welding samples is shown in Figure 9(A), (B), and (C). Figure 9(A) illustrates highest cooling rate achieved in this experimental investigation. The micrograph in Figure 9 displays polygonal ferrite (PF) and widmanstätten ferrite (WF), with bainite and martensite in small amounts. Bainite was observed in the sample that experienced the fastest cooling rate, reaching a maximum joint temperature of 2500°C. This indicates that this specific cooling rate was optimal for achieving the desired microstructure, which is challenging to produce within weld joint microstructure. Tensile test results and microhardness measurements confirmed the favorable bainite formation. When the cooling rate decreases in sample two, which has a maximum expected welding temperature of 2000°C, as shown in Figure 9(B), the weld joint morphology exhibits polygonal ferrite with a significant presence of plate-like martensite and pearlite islands. The quantity of polygonal ferrite varies with changes in the cooling rate, as observed in the last sample. Based on this morphology, the microhardness value of this sample will be higher than that of the first sample with a bainite microstructure due to the extensive formation of martensite plates. The third sample, which reaches a maximum welding temperature of 1800°C, exhibits a reduced cooling rate. This results in a noticeable alteration in the morphology of the welding zone, indicating the initiation of pearlite nucleation and a significant shift in isothermal transformation. The pearlite islands were minuscule and later grew discernible, as seen in Figure 9(C). In this instance, the pearlite islands did not experience growth in size but rather exhibited an increase in quantity.

The microhardness values of the three samples were 252HV for the welding joint with 2500°C, while the microhardness was 221HV for the second sample with 2000°C welding joint temperature and 180 HV for the third sample with 1800°C. The overall pattern indicated a reduction in hardness as the cooling rate dropped [22]. The pace of cooling transitioned rapidly from fast to moderate. The increase in ferrite formation results from more significant quantities due to grain development and recrystallization. This phenomenon is more pronounced when the cooling rates decrease, indicating a transition from diffusion-less to diffusion-controlled transformation. The stability of this process is enhanced when the cooling rates are slower [23]. Another plausible rationale

is that the hardness reaches its maximum level when the martensitic transition is possible at elevated cooling rates. If the martensitic transformation occurs at a slower rate, a more significant amount of retained austenite will be produced. Conversely, if the transformation result is solely bainitic, the creation of retained austenite will decrease. As retained austenite is softer than bainite, this results in a decrease in hardness. When the rate of cooling lowers, the process of bainitic transformation begins. This results in the development of a more significant amount of bainite, which is more complex than retained austenite. Consequently, there is an observed increase in hardness [24].

7.4 Welding joint tensile test results analysis

The tensile test results for the single V joint design at different welding joint temperatures (2500°C, 2000°C, and 1800°C) show that the weldment at 2500°C had the highest ultimate tensile strength of 396.52 MPa, followed by 380.61 MPa at 2000°C, and 344.36 MPa at 1800°C. Based on the investigation mentioned above, it was determined that the single V junction with a higher welding joint temperature exhibits superior ultimate tensile strength compared to the other joints. In this figure, the welding electrode's melting rate, melted base metal quantity, dilution, fusion depth, deposition rates, and penetration depth were appropriate. This indicates that the joint has reached an optimal level of weldability. Furthermore, these findings demonstrate that augmenting the welding current to get this optimal value would increase the wire feed rate and penetration. The failure of all the tensile test samples occurred in heat affected zone (HAZ) due to creating coarse grained zone (CGHAZ) in this area. This structure situated near fusion zone. Temperature range spans from 1100°C to solidus temperature, resulting in significant heat. Specific carbides and nitrides that cannot be dissolved may be dissolved inside the austenite grains, leading to fast growth of the initial austenitic grains. The ϵ -carbides are mainly distributed inside the initial austenitic grains in the Widmanstätten structure, forming a thick overheated structure upon cooling. The material's microstructure is responsible for its apparent anisotropy and low-impact toughness at low temperatures. Additionally, cracks are more likely to form in the area with larger grain size. The overheated zone in welding is considered the weakest point of the welding joint and has been investigated and improved by several researchers [25]. Low temperature impact coarse grain zone toughness in welding heat affected zone significantly reduced. Main reason is quasi-polygonal ferrite and polygonal ferrite microstructures development during thermal welding. The presence of these microstructures causes a disturbance in the anisotropy of the base material and the close-packing acicular ferrite microstructure. Consequently, the CGHAZ (coarse-grained heat-affected zone) becomes fragile, substantially reducing welded joints mechanical characteristics. Steel pipeline welding progress is significantly limited [26]. This phenomenon arises due to the substantial enlargement of the austenite grain with a coarse-grained structure in the region, which is induced by applying heat. As a result, the grain boundary decreases its specific surface area, reducing interfacial energy. This results in a reduction of the density of the grain boundary structure, reducing its inhibitory effect on the movement of dislocations. The elements above all reduce impact toughness at low temperatures and severe embrittlement in the microstructure [27].

7.5 Welding joint microstructure effects on corrosion resistance

Differences in the microstructure have been shown to contribute to variances in general and localized corrosion. Alloy steel with ferrite/pearlite banded structure exhibits good performance regarding localized corrosion. This phenomenon may be ascribed to iron carbide phase segregated distribution known as cementite (Fe_3C) [28]. α -iron and cementite two phase structures create galvanic cells enhance corrosion process, with cementite as cathode. Fine ferrite/pearlite structures exhibited superior performance in corrosion compared to tempered martensite and a banded ferrite/pearlite structure. However, localized corrosion penetration rates similar to tempered martensite [29]. Alloy steel corrosion rate decreases when ferrite proportion rises. This behavior may be explained by the fact that ferrite, which has more iron (Fe) than martensite, functions as anode, while martensite, which has more significant carbon (C) concentration than ferrite, functions as cathode. Based on parameters examined in this work, fine ferrite/pearlite structure, and to some extent coarser ferrite/pearlite structure, may be more appropriate than banded ferrite/pearlite structure. In banded ferrite/pearlite structure, carbon-bearing phase (pearlite) arranged in layers, whereas in other structures, carbon bearing phases dispersed more uniformly [30]. Optimal microstructure for corrosion resistance is achieved by welding conditions that produce a fine ferrite microstructure. This microstructure can be observed in the second sample, which was welded at a temperature of 2000°C. The third sample, welded at 1800°C, exhibits a coarse ferrite with perlite microstructure, less corrosion-resistant. The sample welded at 2500°C, resulting in a Widmanstätten ferrite structure, shows the poorest corrosion resistance.

8. CONCLUSION

Properties related to heat and mechanical behavior of welding alloy steel pipe were carried out. Numerically, the welding process was analyzed with numerical simulations and experimentally welded joint thermal, deformation, microstructure, and mechanical properties characterized and associated with associated heat distribution.

The thermal data revealed that the maximum welding joint heat input across the weldments contributed to the thermal impact. On advancing, the heat input increases the magnitude of weld pool, which, as result, generates wider heat affected zones. Cooling rate relevant to the welding is lower than the heating rate; hence, changes due to the temperature distribution occurred across the alloy. In the welding joint, this value was directly applicable to the heat input ratio; as temperatures rose with the welding, heat affected zone width increased.

Deformation analysis proved that highest deformation was in welding with high welding temperature, and the maximum deformation was at the weld joint end. The welding cooling rate influenced the deformation. Welding process investigated parameters highlighted parameters that resulted in deformation control. It was demonstrated that the reduced welding joint distortion due to the difference in transverse shrinkage mean values over the plate thickness could be achieved by implementing the V-shaped groove angle of 60°.

It was found that the microstructure of the welding joint was affected by the welding cooling rate sampling from the

microstructure analysis. Similarly, bainite was seen for high cooling rates, while polygonal ferrite, martensite, and pearlite phases were induced for lower cooling rates. Martensite formation amount effects can be observed in the recorded microhardness values, showing that larger microhardness is achieved with faster cooling speeds.

The microstructure images give vital information on tensile strength gain at the welding joint. It is essential to mention that in some specimens of the tensile test and heat-affected zone, a disintegration occurred only in coarse grained part. quasi-polygonal and polygonal ferrite microstructural formation configuration to coarse grained zone reduced impact toughness and weakened welded joints' mechanical properties.

Fine ferrite microstructure in 2000°C welding sample shows better corrosion resistance than the welding joint with 1800°C due to the coarse ferrite and perlite structure, and the sample with Widmanstatten ferrite would illustrate the lowest corrosion resistance.

In general, this study provides global insight into alloy steel pipe welding thermal and mechanical properties, same procedure in welding joints, HAZ, and adjacent base metal thermal effects, deformation, and residual stress prediction could be used with the required changes in metal mechanical and physical properties. For future research works the effects of inter-pass temperature or pre-heating and post-heating treatments could be experimentally and numerically investigated. It becomes possible to improve the customer's awareness of the welding process, adapt to welding characteristics, and increase the quality and reliability of welded members.

REFERENCES

- [1] Mohamed, M.S., Abtan, A.A., Moosa, A.U. (2023). Microstructure and mechanical properties assessments of 304 austenitic stainless steel and Monel 400 dissimilar GTAW weldment. *Journal of Composite & Advanced Materials/Revue des Composites et des Matériaux Avancés*, 33(3): 135-144. <https://doi.org/10.18280/rcma.330301>
- [2] DeCost, B.L., Lei, B., Francis, T., Holm, E.A. (2019). High throughput quantitative metallography for complex microstructures using deep learning: A case study in ultrahigh carbon steel. *Microscopy and Microanalysis*, 25(1): 21-29. <https://doi.org/10.1017/S1431927618015635>
- [3] Chiocca, A., Frendo, F., Bertini, L. (2019). Evaluation of heat sources for the simulation of the temperature distribution in gas metal arc welded joints. *Metals*, 9(11): 1142. <https://doi.org/10.3390/met9111142>
- [4] Chiocca, A., Frendo, F., Bertini, L. (2021). Evaluation of residual stresses in a pipe-to-plate welded joint by means of uncoupled thermal-structural simulation and experimental tests. *International Journal of Mechanical Sciences*, 199: 106401. <https://doi.org/10.1016/j.ijmecsci.2021.106401>
- [5] Bhatti, A.A., Barsoum, Z., Murakawa, H., Barsoum, I. (2015). Influence of thermo-mechanical material properties of different steel grades on welding residual stresses and angular distortion. *Materials & Design (1980-2015)*, 65: 878-889. <https://doi.org/10.1016/j.matdes.2014.10.019>
- [6] Hemmesi, K., Farajian, M., Boin, M. (2017). Numerical studies of welding residual stresses in tubular joints and experimental validations by means of x-ray and neutron diffraction analysis. *Materials & Design*, 126: 339-350. <https://doi.org/10.1016/j.matdes.2017.03.088>
- [7] MI, K., ML, K., Biro, E., Zhou, Y. (2008). Microstructure and mechanical properties of resistance spot welded advanced high strength steels. *Materials Transactions*, 49(7): 1629-1637. <https://doi.org/10.2320/matertrans.MRA2008031>
- [8] Hu, J., Du, L. X., Wang, J.J., Gao, C.R. (2013). Effect of welding heat input on microstructures and toughness in simulated CGHAZ of V-N high strength steel. *Materials Science and Engineering: A*, 577: 161-168. <https://doi.org/10.1016/j.msea.2013.04.044>
- [9] Trivedi, A., Chauhan, P. (2011). Modeling of welding heat source for laser spot welding process. In *National Conference on Recent Trends in Engineering & Technology*, BVM Engineering College, VV Nagar, Gujarat, India. https://www.researchgate.net/publication/283299243_Modeling_of_Welding_Heat_Source_for_Laser_Spot_Welding_Process
- [10] Salerno, G., Bennett, C.J., Sun, W., Becker, A.A. (2017). Residual stress analysis and finite element modelling of repair-welded titanium sheets. *Welding in the World*, 61: 1211-1223. <https://doi.org/10.1007/s40194-017-0506-1>
- [11] Zhu, J., Khurshid, M., Barsoum, Z. (2019). Accuracy of computational welding mechanics methods for estimation of angular distortion and residual stresses. *Welding in the World*, 63: 1391-1405. <https://doi.org/10.1007/s40194-019-00746-9>
- [12] Čičo, P., Kalincová, D., Kotus, M. (2011). Influence of welding method on microstructural creation of welded joints. *Research in Agricultural Engineering*, 57: S50-S56. <https://doi.org/10.17221/57/2010-RAE>
- [13] Arora, H., Singh, R., Brar, G.S. (2019). Thermal and structural modelling of arc welding processes: A literature review. *Measurement and Control*, 52(7-8): 955-969. <https://doi.org/10.1177/0020294019857747>
- [14] Abdulameer, A.G., Mohammed, M.S., Abbas, A.S. (2022). Microstructure variation effects influence on characteristics and mechanical properties of Monel 400 and low alloy steel (ASTM 387-Gr. 11) GTAW dissimilar JOINT. *Eastern-European Journal of Enterprise Technologies*, 119(12): 13-20. <https://doi.org/10.15587/1729-4061.2022.266264>
- [15] Grubits, P., Dániel, G., Habashneh, M., Szép, J., Rad, M.M. (2023). Advanced numerical simulation and modeling of welding processes: Stochastic representation of parameters for improved fabrication. *Chemical Engineering Transactions*, 107: 619-624. <https://doi.org/10.3303/CET23107104>
- [16] Moslemi, N., Gohery, S., Abdi, B., Sudin, I., Ghandvar, H., Redzuan, N., Rhee, S. (2022). A novel systematic numerical approach on determination of heat source parameters in welding process. *Journal of Materials Research and Technology*, 18: 4427-4444. <https://doi.org/10.1016/j.jmrt.2022.04.039>
- [17] Dutta, T., Dey, S., Datta, S., Das, D. (2019). Designing dual-phase steels with improved performance using ANN and GA in tandem. *Computational Materials Science*, 157: 6-16. <https://doi.org/10.1016/j.commatsci.2018.10.020>
- [18] Bustamante, C.A., Flórez, W.F., Power, H., Giraldo, M.,

- Hill, A.F. (2010). Control volume-radial basis function method for two-dimensional non-linear heat conduction and convection problems. *Boundary Elements and Other Mesh Reduction Methods XXXII*, 50: 169. <https://doi.org/10.2495/BE1001>
- [19] Derakhshan, E.D., Yazdian, N., Craft, B., Smith, S., Kovacevic, R. (2018). Numerical simulation and experimental validation of residual stress and welding distortion induced by laser-based welding processes of thin structural steel plates in butt joint configuration. *Optics & Laser Technology*, 104: 170-182. <https://doi.org/10.1016/j.optlastec.2018.02.026>
- [20] Rajkumar, N.S., Varma, K.R., Gupta, S., Srihari, T. (2001). A study of effect of groove angle on angular distortion and impact strength in butt welds. In 4th International Conference on Mechanical Engineering, Dhaka, Bangladesh, pp. 26-28. <https://me.buet.ac.bd/public/old/icme/icme2001/cdfiles/Papers/Applied%20Mechanics/serial23.pdf>
- [21] Bachorski, A., Painter, M.J., Smailes, A.J., Wahab, M.A. (1999). Finite-element prediction of distortion during gas metal arc welding using the shrinkage volume approach. *Journal of Materials Processing Technology*, 92: 405-409. [https://doi.org/10.1016/S0924-0136\(99\)00161-2](https://doi.org/10.1016/S0924-0136(99)00161-2)
- [22] Onsøien, M.I., M'hamdi, M., Mo, A. (2009). A CCT diagram for an offshore pipeline steel of X70 type. *Welding Journal*, 88(1): 1s-6s.
- [23] Thompson, S.W., Colvin, D.J., Krauss, G. (1996). Austenite decomposition during continuous cooling of an HSLA-80 plate steel. *Metallurgical and Materials Transactions A*, 27: 1557-1571. <https://doi.org/10.1007/BF02649815>
- [24] Tronskar, J.P. (1995). Evaluation of methods to predict safe welding conditions and maximum HAZ hardness in steel welding. 117(1): 46-56. <https://doi.org/10.1115/1.2826990>
- [25] Moeinifar, S., Kokabi, A.H., Hosseini, H.M. (2011). Role of tandem submerged arc welding thermal cycles on properties of the heat affected zone in X80 microalloyed pipe line steel. *Journal of Materials Processing Technology*, 211(3): 368-375. <https://doi.org/10.1016/j.jmatprotec.2010.10.011>
- [26] Zhang, Y., Zhang, H., Liu, W. (2009). Effects of MA constituent on toughness of coarse grain heat-affected zone in HSLA steels for oil tanks. *Transactions of the China Welding Institution*, 1: 109-112.
- [27] Li, W.W., Liu, Y.X., Gao, H.L., Zhao, X.W., Feng, Y., Ji, L.K. (2006). Analysis of toughness in HAZ for X80 pipeline steel welding. *Transactions of the China Welding Institution*, 2: 43-46.
- [28] Zhang, H., Wang, D., Xue, P., Wu, L.H., Ni, D.R., Ma, Z.Y. (2016). Microstructural evolution and pitting corrosion behavior of friction stir welded joint of high nitrogen stainless steel. *Materials & Design*, 110: 802-810. <https://doi.org/10.1016/j.matdes.2016.08.048>
- [29] Narasaiah, N., Ray, K.K. (2005). Small crack formation in a low carbon steel with banded ferrite-pearlite structure. *Materials Science and Engineering: A*, 392(1-2): 269-277. <https://doi.org/10.1016/j.msea.2004.09.058>
- [30] Clover, D., Kinsella, B., Pejcic, B., De Marco, R. (2005). The influence of microstructure on the corrosion rate of various carbon steels. *Journal of Applied Electrochemistry*, 35: 139-149. <https://doi.org/10.1007/s10800-004-6207-7>